

Higher-Dimensional Topological Insulators in Pure Diffusion Systems

Zhoufei Liu,¹ Liujun Xu,^{1,*} and Jiping Huang^{1,†}

¹*Department of Physics, State Key Laboratory of Surface Physics,
and Key Laboratory of Micro and Nano Photonic Structures (MOE),
Fudan University, Shanghai 200438, China*

(Dated: June 22, 2022)

Abstract

Compared with one dimension, topological insulators (TIs) in higher dimensions contain more unexpected boundary states, such as higher-order topological insulators (HOTIs) that the conventional bulk-boundary correspondence cannot describe. Thanks to the form similarity between the Schrödinger equation and the wave equation, research on HOTIs has been extended from condensed matter to classical wave systems. Unfortunately, it is still challenging to uncover HOTIs in pure diffusion systems because of the essential difference between diffusion and wave. Here, we construct higher-dimensional heat diffusion models based on sphere-rod structures to reveal purely diffusive HOTIs. Starting from two dimensions, we demonstrate diffusive second-order TIs with zero-dimensional corner states and one-dimensional edge states. Unlike Hermitian wave systems, these diffusive boundary states feature the anti-Hermitian dissipative nature and have different decay rates from the bulk states. We further present two-dimensional anisotropic TIs and three-dimensional third-order TIs. Our results open a new gate for diffusive topological states and provide a distinct mechanism for robust boundary heat regulation.

Introduction. Topological states of matter enable the exciting application of dissipationless transport due to their immunity to defects and disorders. Originating from condensed matter physics [1, 2], studies on topological insulators (TIs) have been extended to classical wave systems [3–5] because the wave equation has a similarity to the Schrödinger equation. In dimensions higher than one, TIs exhibit more intriguing boundary states, such as higher-order TIs (HOTIs) [6–14], Chern insulators [15–18], and topological semimetals [19–22]. Uniquely, HOTIs allow topological states with dimensionality two or more lower than that of the system, thus in contrast to conventional first-order TIs.

Beyond waves, diffusion is another crucial mechanism for energy and mass transfer. For flexible heat regulation, thermal metamaterials [23–25] have been designed to realize novel functions, such as cloaking [26–28] and nonreciprocity [29–32]. Nevertheless, robust heat regulation with immunity to defects and disorders remains improved. Recently, the concept of topology has been introduced to heat regulation, facilitating exceptional point/ring encirclements [33–35], robust edge states [36, 37], one-dimensional Su-Schrieffer-Heeger (SSH) models [38–41], and non-Hermitian skin effects [42]. However, most works inevitably require advection to increase the degree of freedom, making it intrinsically elusive to uncover topological states in pure diffusion systems. Another limitation is that existing research mainly focuses on one dimension, hindering those unique diffusive TIs from being revealed in higher dimensions, such as diffusive HOTIs. Therefore, it is extremely inconvenient but urgently necessary to uncover higher-dimensional TIs in pure diffusion systems.

Here, we design higher-dimensional heat conduction models with sphere-rod structures to construct purely diffusive higher-dimensional TIs. Condensed matter physics implies that higher-dimensional SSH models are a kind of HOTIs without multipole moment [8–11]. Resorting to different thermal diffusivity of rods, we present diffusive higher-dimensional SSH models and reveal purely diffusive HOTIs. Specifically, our diffusive two-dimensional SSH models are second-order TIs with zero-dimensional corner states and one-dimensional edge states. These topological corner and edge states are within the gap of bulk states and feature the anti-Hermitian dissipation nature. We analyze the topological invariants based on the topological polarization theory, whose integration region is the whole Brillouin zone. We further construct two-dimensional anisotropic and three-dimensional SSH models to enrich the family of purely diffusive higher-dimensional TIs. Our findings bring new insights into robust heat manipulation and provide a distinct mechanism for heat insulation.

Diffusive two-dimensional SSH model. As shown in Fig. 1(a), we construct a sphere-rod structure in a two-dimensional array, whose density of ρ , heat capacity of c_p , and thermal conductivity of κ are identical. The lengths of the intra-cell and inter-cell rods are the same, and the radii are $R_{0,1}$ and $R_{0,2}$, leading to different thermal diffusivity of D_1 and D_2 . R is the radius of spheres. We realize the fixed boundary condition (FBC) by connecting the boundary rods with constant-temperature heat reservoirs. By discretizing the thermal lattice system, we get an effective Hamiltonian (with dimensionality of 12×12) of the sphere-rod structure, acting as the diffusive counterpart of the two-dimensional SSH model in condensed matter physics. The spectrum of the diffusive two-dimensional SSH model is shown in Fig. 1(b). Compared with wave systems, the present spectrum demonstrates the dissipation nature of our system, and E has the physical meaning of temporal decay rate. Red corner states are in the center of the spectrum, and blue edge states are within the gap. The theoretical eigenstates of the corner and edge states are presented in Figs. 1(c) and 1(d), respectively. Therefore, our sphere-rod structure behaves as a diffusive two-dimensional second-order TI.

Then, we use the periodic boundary condition (PBC), and the Bloch Hamiltonian is

$$\mathcal{H}_{\text{2D SSH}}(\mathbf{k}) = \begin{pmatrix} 2(D_1 + D_2) & -D_1 - D_2 e^{ik_x} & 0 & -D_1 - D_2 e^{ik_y} \\ -D_1 - D_2 e^{-ik_x} & 2(D_1 + D_2) & -D_1 - D_2 e^{ik_y} & 0 \\ 0 & -D_1 - D_2 e^{-ik_y} & 2(D_1 + D_2) & -D_1 - D_2 e^{-ik_x} \\ -D_1 - D_2 e^{-ik_y} & 0 & -D_1 - D_2 e^{ik_x} & 2(D_1 + D_2) \end{pmatrix}, \quad (1)$$

where $D_1 = 3R_{0,1}^2 \kappa / (4R^3 L \rho c_p)$ and $D_2 = 3R_{0,2}^2 \kappa / (4R^3 L \rho c_p)$ are the thermal diffusivity of the rods. Detailed derivations are provided in the Supplemental Material [43]. The Hamiltonian implies that the onsite potentials of the four sublattices are identical, and our diffusive two-dimensional SSH model has only an energy shift compared with the original models in condensed matter physics, which does not affect the topological properties. Specifically, the topological properties are described by the two-dimensional polarization $\mathbf{P} = (P_x, P_y)$,

$$P_j = -\frac{1}{(2\pi)^2} \iint_{\text{BZ}} \hat{\mathcal{A}}_j dk_x dk_y, \quad (2)$$

where $\hat{\mathcal{A}}_j = i \sum_n \langle u_n(k_x, k_y) | \partial_{k_j} | u_n(k_x, k_y) \rangle$ is the Berry connection, n is the occupied band index, $|u_n(k_x, k_y)\rangle$ is the Bloch wave function for the n th band, BZ denotes the Brillouin zone, and $j = x, y$. We use the Wilson loop method to calculate the explicit \mathbf{P} . When $D_1 < D_2$, namely, $\mathbf{P} = (1/2, 1/2)$, the diffusive SSH model is in the topologically nontrivial phase. When $D_1 > D_2$,

namely $\mathbf{P} = (0, 0)$, the model is in the topologically trivial phase. Besides, we define the corner charge Q_c with the nested Wilson loop $p_y^{v_x}$ and $p_x^{v_y}$,

$$Q_c = p_y^{v_x} + p_x^{v_y}. \quad (3)$$

Since there is only one band below the gap, the nested Wilson loop is identical to the Wilson loop. However, this relation is valid only when there are edge states in both x and y directions. Considering these two facts, we get the nested Wilson loop,

$$p_y^{v_x} = p_x^{v_y} = 2P_x P_y. \quad (4)$$

Then, the corner charge is expressed as

$$Q_c = 4P_x P_y. \quad (5)$$

If $\mathbf{P} = (1/2, 1/2)$, we have a corner charge of $Q_c = 1$, indicating that there is one corner state in each of the four corner spheres.

Thermal corner, edge, and bulk states. We further discuss the thermal properties of the diffusive two-dimensional SSH model. The material is stainless steel. We set FBC in x and y directions. We first discuss thermal corner states. Therefore, we set the initial condition by heating the four corner spheres to 333.2 K, and the other spheres and all rods are set at 293.2 K, i.e., the room temperature. The temperature evolution of one corner sphere is shown in Fig. 2(a). The theoretical result is obtained by solving a series of partial differential equations, and the simulated result is obtained by COMSOL Multiphysics. We adopt the logarithmic coordinate. The horizontal axis denotes time t , and the vertical axis denotes $\log[(T - T_f)/(T_i - T_f)]$ with $T_i = 333.2$ K and $T_f = 293.2$ K. The system exchanges heat with the environment and eventually reaches thermal equilibrium. The theoretical and simulated temperature evolutions agree well with each other. Besides, the theoretical temperature evolution in the topologically nontrivial phase follows the line predicted by the corner state. This is a smoking gun of a corner state in the sphere-rod structure. However, the simulated temperature is slightly higher than the theoretical one because heat travels through the rod for a while and then reaches the next sphere in simulations. However, heat instantly travels to the next sphere in theoretical discussions. The theoretical and simulated temperature distributions at $t = 120$ are shown in Figs. 2(b) and 2(c), demonstrating good consistency. Besides, the robustness of corner states against defects is validated in the Supplemental Material [43].

Then, we discuss thermal edge states. The initial condition is realized by heating all edge spheres and rods to 333.2 K. We heat rods to avoid the heat exchange between edge spheres via

rods at the beginning. Otherwise, the temperature decay at edge spheres is very fast. We plot the temperature evolution of the fourth sphere in the unit cell (1, 2). The decay rate of the edge state should be the minimal edge state because the measured temperature mode should have the slowest decay rate. The theoretical and simulated temperature distributions at $t = 180$ s are shown in Figs. 2(e) and 2(f).

We also discuss thermal bulk states. The initial condition is achieved by heating the third sphere in the unit cell (3, 3) to 333.2 K. The theoretical and simulated temperature evolutions on this sphere conform well. The theoretical and simulated temperature distributions at $t = 180$ s are shown in Figs. 2(h) and 2(i).

Anisotropic two-dimensional SSH model. As presented in Fig. 3(a), we further extend the above discussions to an anisotropic two-dimensional SSH model with $R_{0,1x} \neq R_{0,1y}$ and $R_{0,2x} \neq R_{0,2y}$. The two-dimensional polarization is determined by the radii of rods. When $R_{0,1x} < R_{0,2x}$, we get $P_x = 1/2$. If $R_{0,1x} > R_{0,2x}$, we obtain $P_x = 0$. Since the thermal diffusivity is proportional to the square of the rod radius, the relation between thermal diffusivity and two-dimensional polarization is identical to that between the rod radius and polarization. Therefore, we achieve the topological phase diagram of our anisotropic two-dimensional SSH model in Fig. 3(b), classified into four different regions. The two-dimensional polarization is shown in each region. Besides, as explained above, only the phase $\mathbf{P} = (1/2, 1/2)$ has a nonzero corner charge. The phase $\mathbf{P} = (1/2, 0)$ [or $\mathbf{P} = (0, 1/2)$] has only edge states in x (or y) direction. We set $R_{0,1x} < R_{0,2x}$ and $R_{0,1y} > R_{0,2y}$ as an example. The spectrum with FBC is shown in Fig. 3(c), exhibiting only thermal edge states.

We then discuss the thermal properties of the anisotropic SSH model. We consider the case with x direction topologically nontrivial and y direction topologically trivial. We heat all edge spheres and rods in x direction to 333.2 K. The theoretical and simulated temperature evolutions of the fourth sphere in the unit cell (1, 2) are shown in Fig. 3(d), well matching the reference line predicted by the minimal edge state. Then, we heat all edge spheres and rods in y direction to 333.2 K. The theoretical and simulated temperature evolutions of the first sphere in the unit cell (3, 1) are also shown in Fig. 3(d). These results have a significant deviation from the reference line. Therefore, we confirm the existence of an edge state in x direction and the disappearance of an edge state in y direction. The theoretical and simulated temperature distributions at $t = 160$ s are shown in Figs. 3(e) and 3(f) by heating all edge spheres and rods in x direction at the beginning.

Diffusive three-dimensional SSH model. To extend higher-dimensional diffusive TIs, we also construct a diffusive three-dimensional SSH model. We discuss the topologically nontrivial phase,

and the three-dimensional polarization is $\mathbf{P} = (1/2, 1/2, 1/2)$. The diffusive three-dimensional SSH model is a kind of third-order TIs. As shown in Fig. 4(a), thermal corner, hinge, and surface states are found in the spectrum with FBC. The corresponding thermal properties are shown in Figs. 4(b)-4(g). For the corner state, we set the eight corner spheres at 333.2 K as the initial condition, and the temperature distribution at $t = 100$ s is presented in Figs. 4(b) and 4(e). For the hinge state, the initial condition is achieved by heating all hinge spheres and rods to 333.2 K, and the temperature distribution at $t = 120$ s is shown in Figs. 4(c) and 4(f). For the surface state, we heat the surface spheres and rods to 333.2 K, and the temperature distribution at $t = 160$ s is illustrated in Figs. 4(d) and 4(g). Therefore, we confirm our three-dimensional structure is a purely diffusive third-order TIs.

Discussion and Conclusion. We also provide detailed suggestions for experimental demonstration. Since we apply the tight-binding model to explain the topological properties rather than the transfer-matrix method [40], we should make our sphere-rod structures satisfy the fundamental requirements of the tight-binding model in condensed matter physics. Specifically, the tight-binding model requires the hopping amplitude to be as tiny as possible. To this end, we have three comments on experiments. Firstly, the rod radius should be at least twice smaller than the sphere radius. Secondly, the rod length should be no smaller than the sphere radius. Thirdly, the cross-section difference of rods should be more than two times. These settings make our theoretical and simulated results feasible in experiments.

In summary, we have realized higher-dimensional TIs in pure heat conduction systems by constructing diffusive higher-dimensional SSH models. In contrast to one dimension, our diffusive two-dimensional TIs have topological boundary states with dimensionality two lower than that of the system, i.e., diffusive second-order TIs with topological corner states. Theoretical analyses and finite-element simulations confirm thermal corner, edge, and bulk states. We also discuss two-dimensional anisotropic and three-dimensional SSH models for generalization. Our results motivate the exploration of more topological states of matter in pure diffusion systems, such as Weyl semimetals [19], topological superconductors [44], and non-Hermitian TIs [45]. Besides, these exotic topological states help design novel thermal metamaterials for efficient and robust heat manipulation.

Acknowledgments. We acknowledge financial support from the National Natural Science Foundation of China under Grants No. 11725521 and No. 12035004 and the Science and Technology Commission of Shanghai Municipality under Grant No. 20JC1414700.

* 13307110076@fudan.edu.cn

† jphuang@fudan.edu.cn

- [1] M. Z. Hasan and C. L. Kane, *Rev. Mod. Phys.* **82**, 3045 (2010).
- [2] X.-L. Qi and S.-C. Zhang, *Rev. Mod. Phys.* **83**, 1057 (2011).
- [3] T. Ozawa, H. M. Price, A. Amo, N. Goldman, M. Hafezi, L. Lu, M. C. Rechtsman, D. Schuster, J. Simon, O. Zilberberg, and I. Carusotto, *Rev. Mod. Phys.* **91**, 015006 (2019).
- [4] G. C. Ma, M. Xiao, and C. T. Chan, *Nat. Rev. Phys.* **1**, 281 (2019).
- [5] F. Zangeneh-Nejad, A. Alù, and R. Fleury, *C. R. Phys.* **21**, 467 (2020).
- [6] W. A. Benalcazar, B. A. Bernevig, and T. L. Hughes, *Science* **357**, 61 (2017).
- [7] W. A. Benalcazar, B. A. Bernevig, and T. L. Hughes, *Phys. Rev. B* **96**, 245115 (2017).
- [8] B.-Y. Xie, H.-F. Wang, H.-X. Wang, X.-Y. Zhu, J.-H. Jiang, M.-H. Lu, and Y.-F. Chen, *Phys. Rev. B* **98**, 205147 (2018).
- [9] B.-Y. Xie, G.-X. Su, H.-F. Wang, H. Su, X.-P. Shen, P. Zhan, M.-H. Lu, Z.-L. Wang, and Y.-F. Chen, *Phys. Rev. Lett.* **122**, 233903 (2019).
- [10] X. J. Zhang, B.-Y. Xie, H.-F. Wang, X. Y. Xu, Y. Tian, J.-H. Jiang, M.-H. Lu, and Y.-F. Chen, *Nat. Commun.* **10**, 5331 (2019).
- [11] X.-D. Chen, W.-M. Deng, F.-L. Shi, F.-L. Zhao, M. Chen, and J.-W. Dong, *Phys. Rev. Lett.* **122**, 233902 (2019).
- [12] X.-W. Luo and C. W. Zhang, *Phys. Rev. Lett.* **123**, 073601 (2019).
- [13] M. Y. Li, D. Zhirihin, M. Gorlach, X. Ni, D. Filonov, A. Slobozhanyuk, A. Alù, and A. B. Khanikaev, *Nat. Photonics* **14**, 89 (2020).
- [14] B. Y. Xie, H.-X. Wang, X. J. Zhang, P. Zhan, J.-H. Jiang, M. H. Lu, and Y. F. Chen, *Nat. Rev. Phys.* **3**, 520 (2021).
- [15] A. B. Khanikaev, R. Fleury, S. H. Mousavi, and A. Alù, *Nat. Commun.* **6**, 8260 (2015).
- [16] Z. J. Yang, F. Gao, X. H. Shi, X. Lin, Z. Gao, Y. D. Chong, and B. L. Zhang, *Phys. Rev. Lett.* **114**, 114301 (2015).
- [17] Y. J. Ding, Y. G. Peng, Y. F. Zhu, X. D. Fan, J. Yang, B. Liang, X. F. Zhu, X. G. Wan, and J. C. Chen, *Phys. Rev. Lett.* **122**, 014302 (2019).
- [18] A. Souslov, K. Dasbiswas, M. Fruchart, S. Vaikuntanathan, and V. Vitelli, *Phys. Rev. Lett.* **122**, 128001

- (2019).
- [19] N. P. Armitage, E. J. Mele, and A. Vishwanath, *Rev. Mod. Phys.* **90**, 015001 (2018).
 - [20] H.-X. Wang, Z.-K. Lin, B. Jiang, G.-Y. Guo, and J.-H. Jiang, *Phys. Rev. Lett.* **125**, 146401 (2020).
 - [21] B. Jiang, A. Bouhon, Z.-K. Lin, X. X. Zhou, B. Hou, F. Li, R.-J. Slager, and J.-H. Jiang, *Nat. Phys.* **17**, 1239 (2021).
 - [22] L. Luo, H.-X. Wang, Z.-K. Lin, B. Jiang, Y. Wu, F. Li, and J.-H. Jiang, *Nat. Mater.* **20**, 794 (2021).
 - [23] J.-P. Huang, *Theoretical Thermotics: Transformation Thermotics and Extended Theories for Thermal Metamaterials* (Springer, Singapore, 2020).
 - [24] S. Yang, J. Wang, G. L. Dai, F. B. Yang, and J. P. Huang, *Phys. Rep.* **908**, 1 (2021).
 - [25] Y. Li, W. Li, T. C. Han, X. Zheng, J. X. Li, B. W. Li, S. H. Fan, and C.-W. Qiu, *Nat. Rev. Mater.* **6**, 488 (2021).
 - [26] C. Z. Fan, Y. Gao, and J. P. Huang, *Appl. Phys. Lett.* **92**, 251907 (2008).
 - [27] T. Y. Chen, C.-N. Weng, and J.-S. Chen, *Appl. Phys. Lett.* **93**, 114103 (2008).
 - [28] W.-S. Yeung and R.-J. Yang, *Introduction to Thermal Cloaking: Theory and Analysis in Conduction and Convection* (Springer, Singapore, 2022).
 - [29] Y. Li, X. Y. Shen, Z. H. Wu, J. Y. Huang, Y. X. Chen, Y. S. Ni, and J. P. Huang, *Phys. Rev. Lett.* **115**, 195503 (2015).
 - [30] D. Torrent, O. Poncelet, and J. C. Batsale, *Phys. Rev. Lett.* **120**, 125501 (2018).
 - [31] M. Camacho, B. Edwards, and N. Engheta, *Nat. Commun.* **11**, 3733 (2020).
 - [32] L. J. Xu, G. Q. Xu, J. P. Huang, and C.-W. Qiu, *Phys. Rev. Lett.* **128**, 145901 (2022).
 - [33] L. J. Xu, J. Wang, G. L. Dai, S. Yang, F. B. Yang, G. Wang, and J. P. Huang, *Int. J. Heat Mass Transf.* **165**, 120659 (2021).
 - [34] G. Q. Xu, Y. Li, W. Li, S. H. Fan, and C.-W. Qiu, *Phys. Rev. Lett.* **127**, 105901 (2021).
 - [35] G. Q. Xu, W. Li, X. Zhou, H. G. Li, Y. Li, S. H. Fan, S. Zhang, D. N. Christodoulides, and C.-W. Qiu, *Proc. Natl. Acad. Sci. U. S. A.* **119**, e2110018119 (2022).
 - [36] L. J. Xu and J. P. Huang, *EPL* **134**, 60001 (2021).
 - [37] G. Q. Xu, Y. H. Yang, X. Zhou, H. S. Chen, A. Alù, and C.-W. Qiu, *Nat. Phys.* **18**, 450 (2022).
 - [38] T. Yoshida and Y. Hatsugai, *Sci. Rep.* **11**, 1 (2021).
 - [39] S. Makino, T. Fukui, T. Yoshida, and Y. Hatsugai, *Phys. Rev. E* **105**, 024137 (2022).
 - [40] M. H. Qi, D. Wang, P.-C. Cao, X.-F. Zhu, C.-W. Qiu, H. S. Chen, and Y. Li, *Adv. Mater.* , 2202241 (2022).

- [41] H. Hu, S. Han, Y. H. Yang, D. J. Liu, H. R. Xue, G.-G. Liu, Z. Y. Cheng, Q. J. Wang, S. Zhang, B. L. Zhang, and Y. Luo, *Adv. Mater.* , 2202257 (2022).
- [42] P.-C. Cao, Y. Li, Y.-G. Peng, M. H. Qi, W.-X. Huang, P.-Q. Li, and X.-F. Zhu, *Commun. Phys.* **4**, 230 (2021).
- [43] See Supplemental Material, which includes Ref. [40].
- [44] M. Sato and Y. Ando, *Rep. Prog. Phys.* **80**, 076501 (2017).
- [45] Y. Ashida, Z. P. Gong, and M. Ueda, *Adv. Phys.* **69**, 249 (2020).

FIGURE CAPTION

Fig. 1. Diffusive two-dimensional SSH model. (a) Schematic diagram of the sphere-rod structure with four constant-temperature boundaries set at 293.2 K (i.e., fixed boundary condition, FBC). Black circles denote spheres. Blue and orange lines denote rods with diffusivity of D_1 and D_2 . The central dashed square shows a unit cell, where the numbers label the four sublattices. (b) Spectrum of the model with FBC. Red dots, blue stars, and green squares denote thermal corner, edge, and bulk states. The theoretical eigenstate of (c) the corner state and (d) the lower branch edge state in Fig. 1(b). The parameters are $D_1 = 2.4 \times 10^{-3} \text{ m}^2/\text{s}$ and $D_2 = 9.6 \times 10^{-3} \text{ m}^2/\text{s}$. The unit cell number is $6 \times 6 = 36$.

Fig. 2. Thermal corner, edge, and bulk states. Temperature evolution of (a) the corner state, (d) the edge state, and (g) the bulk state. Theoretical and simulated temperature distributions of (b) and (c) the corner state at $t = 120 \text{ s}$ (nontrivial phase), (e) and (f) the edge state at $t = 180 \text{ s}$ (nontrivial phase), and (h) and (i) the bulk state at $t = 180 \text{ s}$ (nontrivial phase). The parameters are $R = 5 \text{ mm}$, $L = 10 \text{ mm}$, $\kappa = 16 \text{ W m}^{-1} \text{ K}^{-1}$, $\rho = 8000 \text{ kg/m}^3$, $c_p = 500 \text{ J kg}^{-1} \text{ K}^{-1}$. $R_{0,1} = 1 \text{ mm}$ and $R_{0,2} = 2 \text{ mm}$ for the nontrivial phase. $R_{0,1} = 2 \text{ mm}$ and $R_{0,2} = 1 \text{ mm}$ for the trivial phase.

Fig. 3. Anisotropic two-dimensional SSH model. (a) Schematic diagram. Different colored lines denote rods with diffusivity of D_{x1} , D_{x2} , D_{y1} , and D_{y2} . (b) Phase diagram with the two-dimensional polarization of $\mathbf{P} = (P_x, P_y)$. (c) Spectrum of the model with FBC. The blue stars and green squares denote the edge and bulk states, respectively. (d) Temperature evolution of the edge state. (e) and (f) Theoretical and simulated temperature distributions of the edge state at $t = 160 \text{ s}$ (nontrivial phase). The parameters are $R_{0,1x} = 1 \text{ mm}$, $R_{0,2x} = 2 \text{ mm}$, $R_{0,1y} = 2 \text{ mm}$, and $R_{0,2y} = 1 \text{ mm}$. The other parameters are the same as those in Fig. 2.

Fig. 4. Diffusive three-dimensional SSH model. (a) Spectrum of the model with FBC. The red circles, blue stars, orange triangles, and green squares denote thermal corner, hinge, surface, and bulk states, respectively. Theoretical and simulated temperature distributions of (b) and (e) the corner state at $t = 100 \text{ s}$, (c) and (f) the hinge state at $t = 120 \text{ s}$, and (d) and (g) the surface state at $t = 160 \text{ s}$. The parameters are $R_{0,1x} = R_{0,1y} = R_{0,1z} = 1 \text{ mm}$ and $R_{0,2x} = R_{0,2y} = R_{0,2z} = 2 \text{ mm}$. The other parameters are the same as those in Fig. 2.

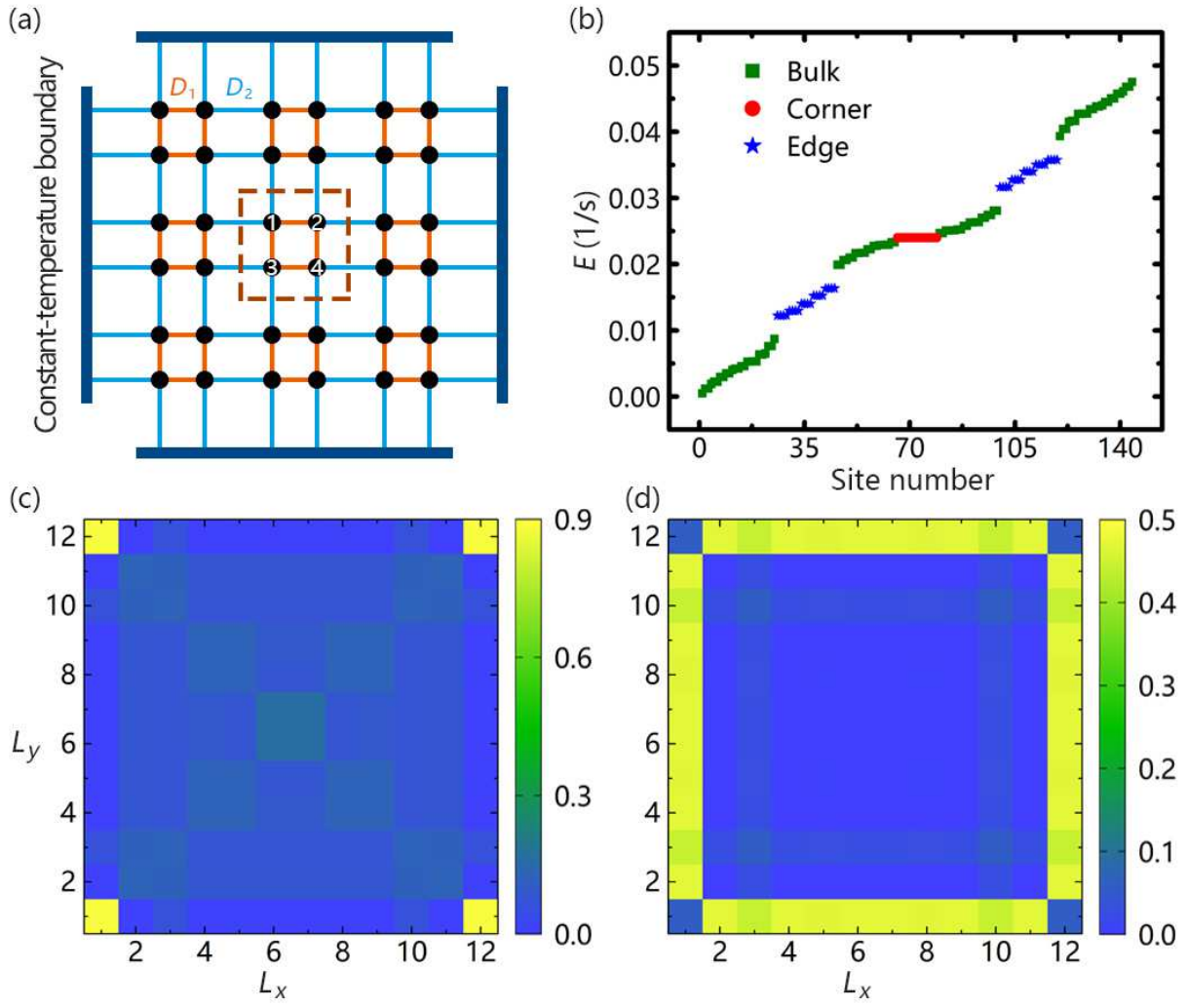


FIG. 1. Liu, Xu, and Huang

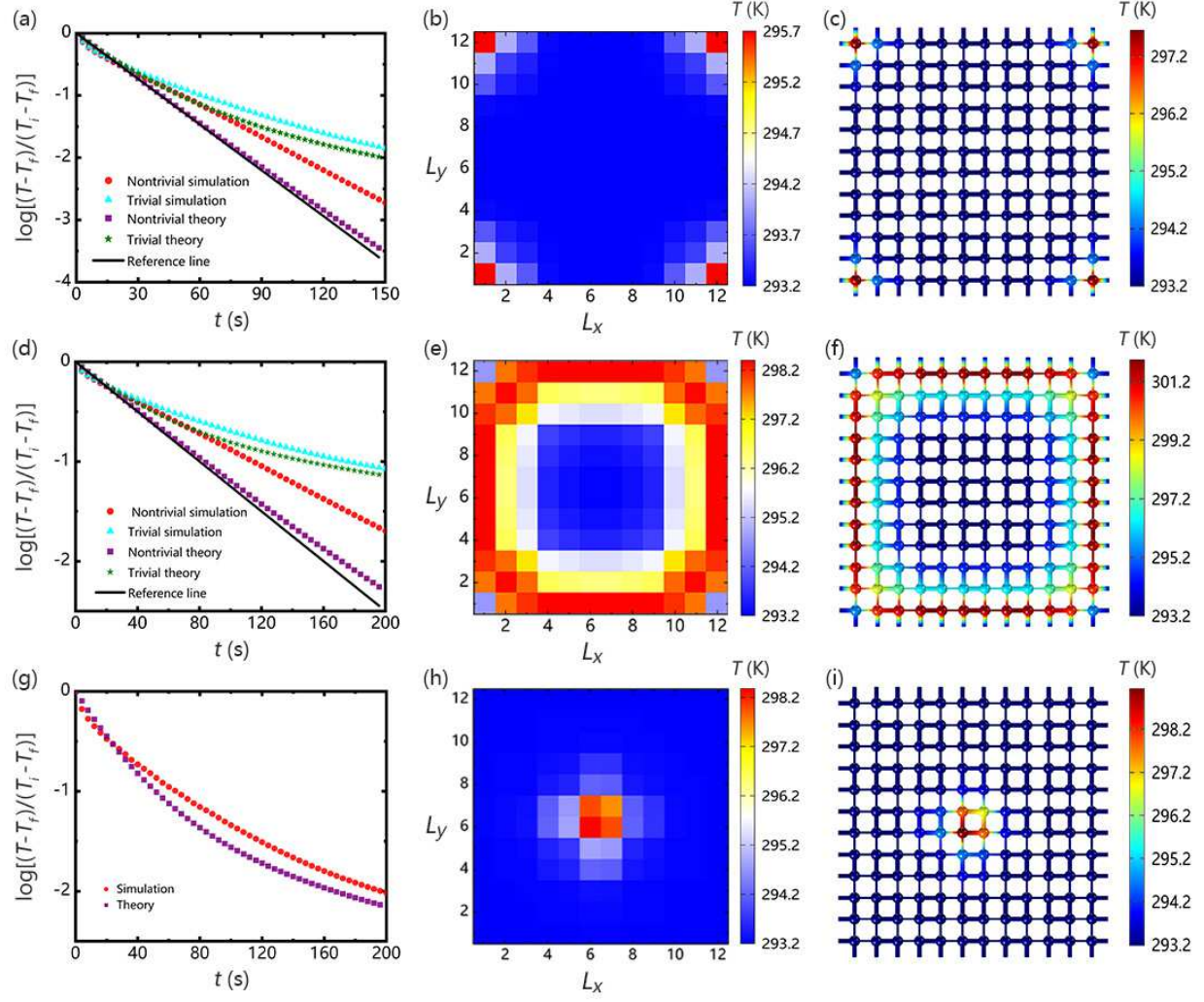


FIG. 2. Liu, Xu, and Huang

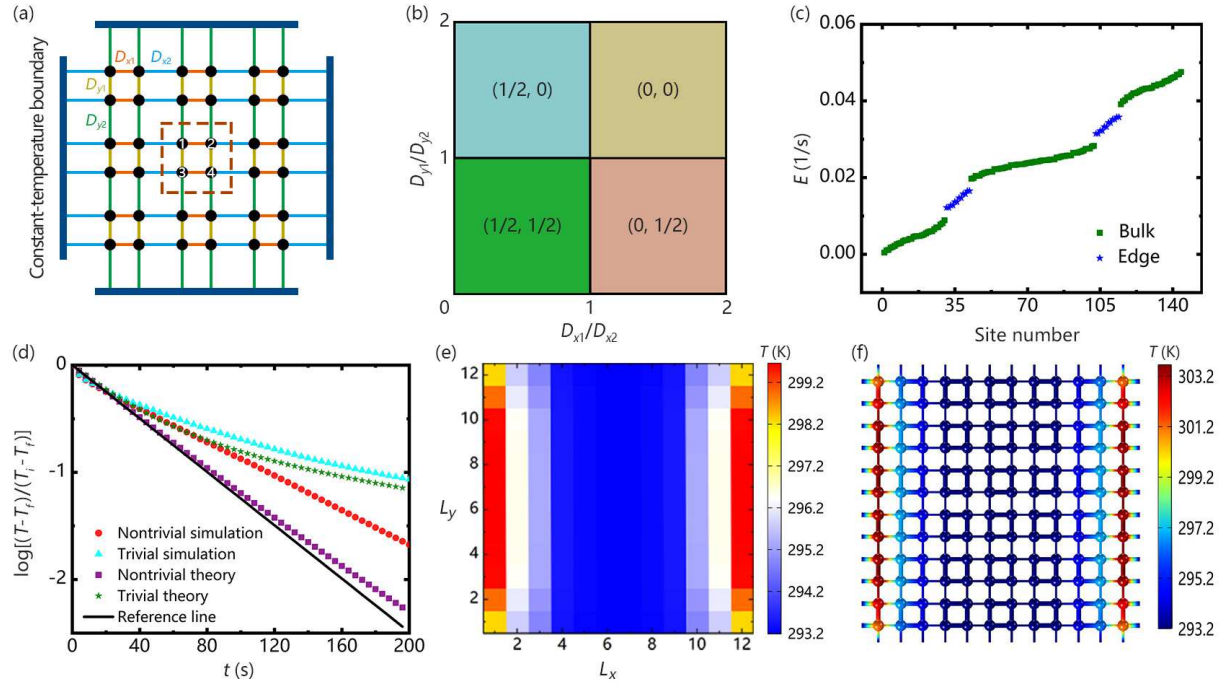


FIG. 3. Liu, Xu, and Huang

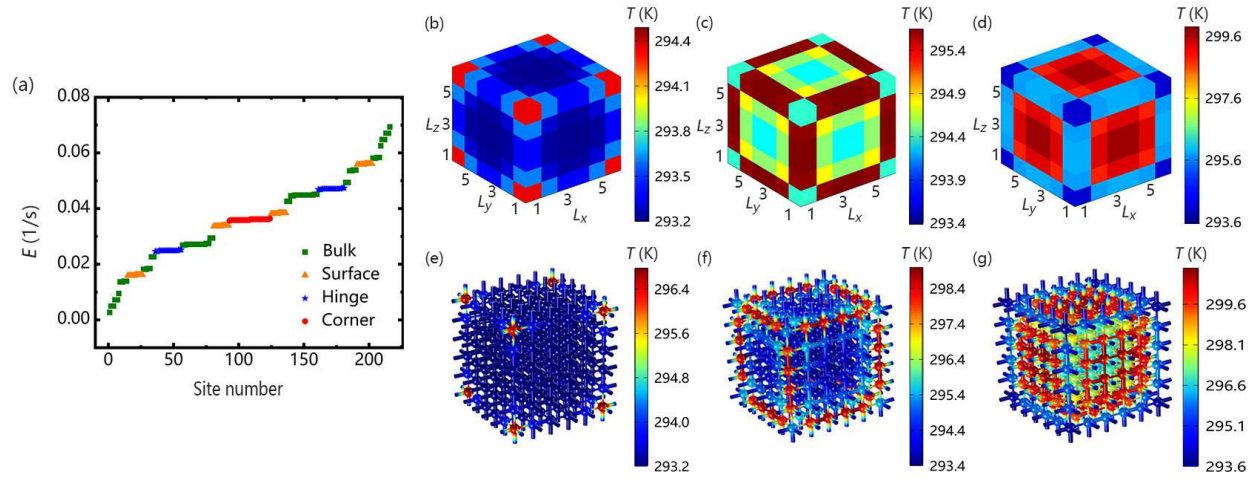


FIG. 4. Liu, Xu, and Huang